A Dynamical Model of Rocket Propellant Loading with Liquid Hydrogen

Viatcheslav V. Osipov[1]
MCT, Inc., NASA Ames Research Center, Moffett Field, CA, 94035, USA

Matthew J. Daigle[2]
University of California, Santa Cruz, NASA Ames Research Center, Moffett Field, CA, 94035, USA

Cyrill B. Muratov[3]
NASA Ames Research Center, Moffett Field, CA 94035,

New Jersey Institute of Technology, Newark, NJ, 07102, USA

Michael Foygel[4]
South Dakota School of Mines and Technology, Rapid City, SD, 57701, USA

Vadim N. Smelyanskiy[5]
NASA Ames Research Center, Moffett Field, CA, 94035, USA

Michael D. Watson[6]
NASA Marshall Space Flight Center, Huntsville, AL, 35805 USA

---

[1] Leading Researcher, MCT, Inc., NASA Ames Research Center, Moffett Field, CA, 94035, USA.
[2] Associate Scientist, Intelligent Systems Division, NASA Ames Research Center, Moffett Field, CA 94035, USA. AIAA Member.
[3] Associate Professor, Department of Mathematical Sciences, New Jersey Institute of Technology, Newark, NJ, 07102, USA.
[4] Professor, Physics Department, South Dakota School of Mines and Technology, Rapid City, SD, 57701, USA.
[5] Senior Research Scientist, Applied Physics Group Lead, NASA Ames Research Center, Moffett Field, CA 94035, USA.
[6] Chief, ISHM and Sensors Branch, NASA Marshall Space Flight Center, Huntsville, AL, 35805, USA.

A dynamical model describing the multi-stage process of rocket propellant loading has been developed. It accounts for both the nominal and faulty regimes of cryogenic fuel loading when liquid hydrogen is moved from a storage tank to an external tank via a transfer line. By employing basic conservation laws, the reduced, lumped-parameter model takes into consideration the major multi-phase mass and energy exchange processes involved, such as highly non-equilibrium condensation-evaporation of hydrogen, pressurization of the tanks, and liquid hydrogen and hydrogen vapor flows in the presence of pressurizing helium gas. A self-consistent theory of dynamical condensation-evaporation has been developed that incorporates heat flow by both conduction and convection through the liquid-vapor interface inside the tanks. A simulation has been developed in Matlab for a generic refueling system that involves the solution of a system of ordinary integro-differential equations. The results of these simulations are in good agreement with the Space Shuttle refueling data.

Nomenclature

Subscripts

a	= refers to ambient
$boil$	= related to vapor generated by vaporizer
C	= refers to critical point
e	= refers to external heat or mass flows across the control volume
	boundaries other than liquid/vapor interface
f	= refers to gaseous hydrogen vapor film
lv	= refers to liquid/vapor phase transition
g	= refers to gaseous helium
i	= 1 refers to storage tank
i	= 2 refers to external tank
k	= enumerates elements of transfer line or valves
l	= refers to liquid hydrogen
$leak$	= refers to leaks
ls	= refers to saturated liquid
$pipe$	= refers to pipe
S	= refers to liquid/vapor interface
tr	= refers to transfer line
v	= refers to gaseous hydrogen vapor
$valve$	= refers to valves
vap	= refers to vaporizer
vs	= refers to saturated vapor
w	= refers to tank wall
$w/boil$	= related to vapor generated by tank walls

Dynamical Variables

h_l = height (level) of liquid; m

J = gas/vapor or liquid mass flow rate; kg/s

m = mass of a control volume; kg

p = (partial) pressure; Pa

$\dot{Q}$ = heat flow rate from or to a control volume; W

T = temperature; K

V = volume; m^3

$\dot{W}$ = power on or by a control volume; W

ρ = density; kg/m^3

Liquid/Vapor Parameters

$c_{P(V)}$ = constant pressure (volume) specific heat; J/K·kg

h = specific enthalpy; J/kg

Nu, Ra, Re, Pr = dimensionless Nusselt, Rayleigh, Reynolds, and Prandtl numbers

R_v, R_g = LH2 and GHE gas constants; J/K·kg

u = specific internal energy; J/kg

α = convection heat transfer coefficient; W/m^2·K

γ = ratio of specific heats; c_P/c_V

κ = thermal conductivity; W/m·K

μ = dynamic viscosity; kg/m·s

ν = kinematic viscosity; m^2/s

Filling System Parameters

A = cross-sectional area of ST, pipe, or liquid/vapor interface in storage tank; m^2

d_r = wall roughness; m

f = dimensionless resistance coefficient

H = height of external tank; m

K = dimensionless loss factor

l = pipe length; m

R = radius of external tank, storage tank, or a pipe; m

S = cross-sectional area of vent valve area or leak hole; m^2

v = velocity of liquid/vapor in tubes or valves; m/s

λ = dimensionless vent valve position

σ = dimensionless multiplicative clogging factor

τ = time constant of vaporizer valve or transfer line; s

I. Introduction

The fueling of rockets with liquid propellant is a very important and dangerous procedure, especially in the case of hydrogen [1–4]. The major goal of this paper is to develop a medium-fidelity, lumped-parameter dynamical model of propellant loading that (*i*) takes into consideration a variety of complex multi-phase phenomena that govern the storage and transfer of cryogenic propellants, and yet is simple enough to (*ii*) allow for physics analysis and is suitable for numerical simulations of real loading systems. With relatively small modifications, the proposed model can be applied to the description of on-ground loading of different cryogenic propellants and account for thermal stratification in the ullage regions of the tanks. In this paper, we concentrate on a system of liquid hydrogen (LH2) filling motivated by the parameters of the Space Shuttle refueling system. Such a system can be considered as generic with respect to many existing and emerging liquid propellant loading schemes and cryogenic fluid management technologies.

The purpose of the LH2 propellant loading system is to move LH2 from the storage tank (ST) to the external tank (ET) (see Fig. 1). LH2 is stored on the ground in a spherical, insulated, double-walled storage tank with a radius of about ten meters. The height of the ET is about thirty meters. The corresponding
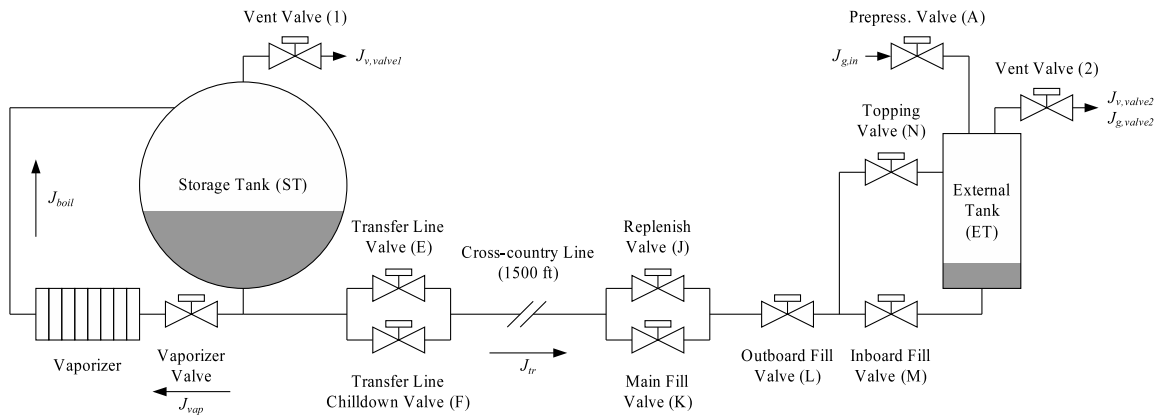
Fig. 1 LH2 propellant loading schematic.

hydrostatic pressure of liquid hydrogen near the bottom of the tanks is much less than the saturated vapor pressure at the operating temperature. Therefore, a high operating pressure is needed to suppress potential boiling of the liquid hydrogen. To ensure such pressure, helium gas is injected into the ET, and pressure is maintained throughout filling with the help of a vent valve. In the ST, a vaporizer is used to maintain the ullage pressure by producing gaseous hydrogen (GH2). It is kept at a higher pressure than in the ET such that the transfer of LH2 from the ST into the ET is accomplished.

An accurate model of this system is needed for supporting loading procedure optimization analyses and ensuring system safety through model-based fault diagnostic and prognostic algorithms. However, developing such a model, especially one that is simple, yet accurate enough for these purposes, is challenging: though complex physics phenomena govern the flow of the cryogenic propellants, only limited data is available to validate models. The processes of heat transfer and phase change prove to be central to the understanding of the loading system and its correct functioning [1, 4]. In [1], while describing a cryogenic (external) tank history, Estey *et al.* took into consideration heat transfer by convection only. In some cases, however, the heat transfer by conduction is essential in the treatment of the heat and mass flow across the LH2/GH2 boundary leading to the so-called condensation blocking [4]. The latter effect is shown [4] to be essential to the consistent description of the cryogenic tank history.

The paper is organized in the following way. In Section II we consider the non-equilibrium dynamics of condensation-evaporation at, and of the heat flow through, the liquid/vapor interface. Section III deals with a consistent description of the cryogenic tank's history. It incorporates the analysis of the propellant mass flow
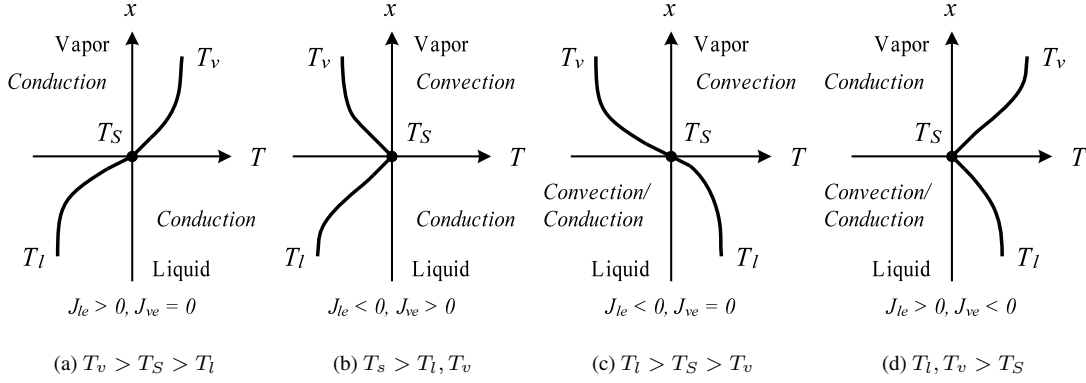
Fig. 2 Interfacial heat exchange modes in a propellant tank.

in the transfer line, which is critical to an adequate modeling of the nominal and the faulty regimes of the rocket propellant loading, described in Sections IV and V, respectively. In Section VI, the model is validated against data collected from a real rocket cryogenic (LH2) propellant loading system. Section VII concludes the paper.

II. Condensation-evaporation and Heat Flow Processes

We begin with a general description of the condensation-evaporation and heat flow, that occurs at the LH2/GH2 interface, as these processes form the core of the propellant loading model. If, in a tank partially filled by a cryogenic propellant, the liquid phase is in thermodynamic equilibrium with the vapor phase above it, then the temperature profile is uniform across the interface. The mass flow rate due to condensation J_c is balanced by the evaporation mass flow rate J_d so that both the net mass flow rate $J_{lv} = J_c - J_d$ from the vapor control volume (CV) to the liquid CV and the heat flow through the liquid/vapor interface disappear. When the tank is being filled or emptied, $J_{lv} \neq 0$. As evaporation is accompanied by heat removal it leads to cooling of the interface, while condensation results in its heating. Therefore, in non-equilibrium conditions the interface temperature T_S differs from that of the bulk liquid, T_l, and that of the vapor, T_v, resulting in temperature gradients in both the liquid and vapor volumes adjacent to the interface, as shown in Fig. 2, in which possible operational modes are indicated that can be responsible for the shown sequence of temperatures, and positive external flow rates $J_{el(v)}$ correspond to mass entering CV $l(v)$. In turn, these gradients will generate non-vanishing heat fluxes $\dot{Q}_v$ and $\dot{Q}_l$ across the interface. Depending on the situation, these fluxes can be associated with heat transfer due to conduction or natural convection [4].

7

Our estimates show that if the processes involved vary slowly over time scales exceeding 0.1 seconds, then the natural convection, if present, dominates the heat conduction in GH2 at low temperatures. (The heat transfer from the tank walls will further facilitate the effect of convection.) Then, taking into consideration that natural convection can occur if the lower part of a CV, liquid or vapor, is hotter than the upper one, we have derived the classification of temperature gradients and of the heat transfer regimes in the vicinity of the liquid/vapor interface, shown in Figure 2.

If heat is transferred to or from the interface ($x = 0$) due to conduction, its flow through the interface is defined by the temperature gradient in the direction normal to the interface [5]:

$$\dot{Q}_{l(v)}(t) = -\kappa_{l(v)} A \left. \frac{\partial \Theta(x, t)}{\partial x} \right|_{x=0}. \tag{1}$$

In this case, given the initial homogeneous temperature $\Theta(x, t = 0) = T_{l(v)}$, the interface temperature $T_S(t) = \Theta(x = 0, t)$ can be expressed in terms of the heat flow rate $\dot{Q}_{l(v)}$ as follows [4, 5]:

$$T_S(t) = \Theta(0, t) = \frac{1}{A\sqrt{\pi c_{l(v)} \rho_{l(v)} \kappa_{l(v)}}} \int_0^t d\tau \frac{\dot{Q}_{l(v)}(\tau)}{(t - \tau)^{1/2}} + T_{l(v)}. \tag{2}$$

The latter, in turn, is related to the net condensation-evaporation mass flow through the interface associated with the latent heat generated at, or absorbed by, the interface.

Taking into account the microscopic Hertz-Knudsen relation [5] for the condensation-evaporation fluxes, it is possible [4] (*i*) to relate the interface temperature to the vapor pressure and (*ii*) to prove that the pressure at the LH2/GH2 interface is close to that of saturated LH2 vapor taken at the interface temperature T_S. In other words, in spite of highly non-equilibrium conditions in the tank, quasi-equilibrium takes place at the LH2/GH2 interface as a result of the so-called dynamical condensation blocking effect [4]. It can be explained as follows. Due to LH2's low thermal conductivity, the LH2/GH2 interface temperature, depending on the situation, either rises or drops due to the condensation-evaporation latent heat released or absorbed at the interface until the condensation mass flow rate nearly compensates the evaporation mass flow rate. These considerations allow us to introduce a very thin, massless, saturated vapor film CV (f) (Fig. 2) that separates the vapor/gas CV (v) from that of the liquid (l) (see also Estey *et al.* [1]). The temperature across this thin film, T_f, is considered uniform and set to be equal to T_S.

In these circumstances, the most natural and simple way of treating the interface heat exchange is by means of reversing Eq. (2), so that the heat flow rate due to conduction is related to the time variations of the

interface temperature as follows [5]:

$$\dot{Q}_{l(v)}^{cond}(t) = A \left(\frac{\kappa_{l(v)} c_{l(v)} \rho_{l(v)}}{\pi} \right)^{1/2} \int_0^t \frac{d\tau}{(t-\tau)^{1/2}} \frac{\partial T_S(\tau)}{\partial \tau}. \tag{3}$$

If the heat transfer is dominated by convection, then

$$\dot{Q}_v^{conv} = A\alpha_v(T_S - T_v)H(T_S - T_v) \tag{4}$$

$$\dot{Q}_l^{conv} = A\alpha_l(T_l - T_S)H(T_l - T_S), \tag{5}$$

where the Heaviside function H takes care of the proper temperature conditions required for convection. (The convection heat transfer coefficients are given in Appendix A.) In general, the heat transfer rate from the bulk of the corresponding CV to the interface or vice versa can be calculated as

$$\dot{Q}_{l(v)} = \pm \max \left\{ \dot{Q}_{l(v)}^{cond}, \dot{Q}_{l(v)}^{conv} \right\} \tag{6}$$

Here, a $+$ is chosen when $T_v > T_S$ or $T_S > T_l$, and a $-$ otherwise. It should be noted that in (3), (4), and (5) the temperature evolution T_S is defined by the vapor and liquid variables far from the interface. These, in turn, are partially defined by the interface heat flow rates (6) in a self-consistent manner. In addition, the total heat flow through the LH2/GH2 interface defines the condensation-evaporation mass flow rate.

III.   Description of the Model

In each tank partially filled with liquid hydrogen and a mixture of gaseous hydrogen and possibly another gas, usually helium (Fig. 3), we will consider three control volumes: the vapor, the liquid, and the vapor film, each treated by means of the lumped parameter method.

A.   Equations of State

The vapor CV (v) is treated as a mixture of ideal gases with time dependent partial densities $\rho_{v(g)}$ and pressures $p_{v(g)}$, as well as a common temperature T_v, all related to each other by two independent equations of state

$$p_{v(g)} = \rho_{v(g)} R_{v(g)} T_v \tag{7}$$

The total pressure $p_t = p_v + p_g$. (In the absence of GHe, $\rho_g = 0$.)
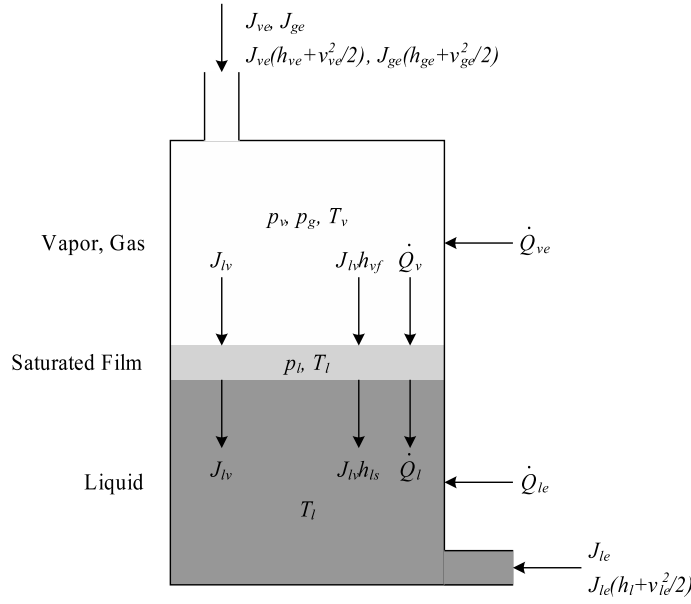
9

Fig. 3 Control Volumes (CV), mass and energy flows in an LH2 tank.

The liquid CV (l) is where, far from the surface, the temperature is equal to T_l and the liquid is treated as incompressible.

The vapor film CV (f) separates the liquid and gas phases. It is treated as saturated hydrogen vapor, whose temperature is equal to that of the interface, where [1, 4, 6]

$$p_f(T_f) = p_C \left(T_f/T_C\right)^n ,$$

(8)

with $p_C = 1.315$ MPa, $T_C = 33.2$ K, and $n = 5$ for hydrogen [6]. (To relate p_f to $T_f = T_S$ one can also use the Antoine equation [7, 8].) We consider the filling process to be slow enough so that at every instant of time the pressure is constant across all the CVs, and $p_v = p_f$. Meanwhile, the temperature is treated as varying from T_l to T_v in the direction x perpendicular to the interface (Fig. 2).

B. Mass Conservation

For the liquid CV, the mass conservation is defined by the external mass flow (i.e., the flow across its boundaries other than through the v/l interface), which is considered negative for fluid removal, and the interphase (condensation-evaporation) flow as follows (Fig. 2):

$$\dot{m}_l = J_l = \rho_l \frac{dV_l}{dt} = J_{le} + J_{lv}$$

(9)

10

Similarly, due to the absence of GHe flux into the liquid CV, the GH2 and GHe mass conservation for CV (v) yields (see Fig. 2) :

$$\dot{m}_v = \frac{d\,(\rho_v V_v)}{dt} = (V - V_l)\frac{d\rho_v}{dt} - \rho_v \frac{dV_l}{dt} = J_{ve} - J_{lv} \tag{10}$$

$$\dot{m}_g = \frac{d\,(\rho_g V_v)}{dt} = (V - V_l)\frac{d\rho_g}{dt} - \rho_g \frac{dV_l}{dt} = J_{ge} \tag{11}$$

where, for the sake of consistency, the net interphase mass flow is taken with a "$-$" sign. Here, we take into consideration that for a given tank volume V, the vapor volume is fully defined by either the liquid CV volume or its mass:

$$V = V_v + V_l = V_v + m_l/\rho_l \tag{12}$$

C. Energy Conservation

The energy conservation for the vapor CV is:

$$\dot{Q}_{ve} - \dot{Q}_v - \dot{W} - J_{lv}h_{vs} + J_{ve}(h_v + v_{ve}^2/2) + J_{ge}(h_g + v_{ge}^2/2) = \frac{d(m_v u_v + m_g u_g)}{dt} \tag{13}$$

where $\dot{Q}_{ve}$ is the net external heat flow into the CV (v) through the tank walls, and the heat flow leaving the CV (v) through the v/f interface, $\dot{Q}_v$, is given by Eq. (6).

The flow of specific enthalpy, $J_{lv}h_{vs}$ in (13), describes the flow of energy leaving the CV (v) through the v/f interface due to the condensation-evaporation mass flow, if its kinetic energy is being ignored. (Since this flow is carried by the *saturated* vapor, its specific enthalpy is equal to h_{vs}.) The transfer of energy due to external GH2 mass flow is described by the $J_{ve}(h_v + v_{ve}^2/2)$ terms [5]. Here, the kinetic energy associated with both the GH2 mass flow entering the CV (v) are taken into consideration, because the corresponding velocities $v_{ve} = J_{ve}/\rho_v A_{ve}$ are much greater than the one related to interphase flow. The term $\dot{W} = -p_t dV_l/dt$ is related to the quasi-static power due to compression (expansion) of the CV (v). The specific internal ideal gas energies on the right side of Eq. (13) $u_v = c_{V,v}T_v$, while the specific enthalpies $h_v = u_v + p_v/\rho_v = u_v + R_v T_v = c_{P,v}T_v$. Here, $c_{P,v} = c_{V,v} + R_v$. Corresponding equations hold also for the GHe mass flow entering the CV, where subscript v should be substituted with g.

If the film layer is considered negligibly thin so that one can ignore its mass (for clarifications, see Estey *et. al.* [1] and Section II), then the energy balance equation for the CV (f) can be written as

$$\dot{Q}_v - \dot{Q}_l + J_{lv}(h_{vs} - h_{ls}) = \frac{d(m_f u_f)}{dt} = 0, \tag{14}$$

where at the f/l (v/f) interface, the liquid (vapor) is considered saturated with $h = h_{ls}(h_{vs})$.

Here, the specific enthalpy of the saturated hydrogen vapor (liquid), $h_{vs(ls)}$, is taken at a film temperature equal to that of the surface of the liquid: $T = T_f = T_S$, so that the specific enthalpy (heat) of vaporization $h_{lv}(T_f) = h_{vs} - h_{ls}$, strictly speaking, depends on the saturated vapor temperature: it goes to zero when the surface temperature approaches the critical temperature T_C [7, 8]. To take this effect into consideration, we will use the following simple interpolation formula for $T_f = T_S \leq T_C$:

$$h_{lv}(T_f) = h_{lv}^0 \left(\frac{T_C - T_f}{T_C - T_l(0)} \right)^{1/2}, \tag{15}$$

where for liquid hydrogen, $T_C = 33$ K and $h_{lv}^0 \cong u_{lv}^0 = 4.5 \times 10^5$ J/kg at $p = 1$ atm and $T_l(0) = 20$ K [7, 8].

In order to relate the temperature of the liquid, T_l, to the external mass flow and the condensation-evaporation mass flow as well as to the energy flows to or from the CV (l), the above equations should be complemented with the energy conservation for the liquid CV (l):

$$\dot{Q}_{le} + \dot{Q}_l + \dot{W} + J_{lv}h_{ls} + J_{le}(h_l + v_{le}^2/2) = \frac{d(m_l u_l)}{dt}, \tag{16}$$

where the specific enthalpy of liquid is considered to be proportional to its temperature: $h_l \cong u_l \cong c_l T_l$.

Both the liquid and vapor CVs absorb external (e) heat from the tank walls (see Eqs. (13) and (16)). This heat is transferred by means of convection so that

$$\dot{Q}_{v(l)e} = A_{v(l)} \alpha_{v(l)e} \left(T_w - T_{v(l)} \right), \tag{17}$$

where the convection heat transfer coefficients are evaluated in Appendix A. In (17), the wall temperature T_w is governed by the heat flow passing through the walls from the environment [1–3]. Also, here $A_{v(l)}$ are the internal tank surfaces in contact with vapor (liquid) (see Appendix A).

The temperature T_w, considered uniform, of the tank wall is to be defined by the heat exchange rate with the tank surroundings with the effective ambient temperature T_a:

$$\dot{Q}_w = A \alpha_w \left(T_a - T_w \right). \tag{18}$$

The wall temperature is governed by the tank energy conservation [1]:

$$m_w c_w \dot{T}_w = \dot{Q}_w - \dot{Q}_{le} - \dot{Q}_{ve}. \tag{19}$$

Here, the heat transfer coefficients (see Appendix A) describe natural convection inside and outside the tank walls [1, 9]. (In the case of heat exchange with the surroundings driven by radiation, $\dot{Q}_w$ represents the radiation heat flow rate [9].)

D. The Storage Tank

To apply the above equations (3)–(19) to the description of the storage tank (ST) history, we have to associate them with variables, parameters, and functions related to the ST. First, we will ascribe a subscript $i = 1$ to all of them. Second, we will specify some of the mass and energy flow rates.

There is no GHe in the ullage volume of the ST, so we will put everywhere $p_{g1} = \rho_{g1} = 0$. Also, we specify the external liquid-mass flow rate in Eq. (9) as follows. For the ST (see Fig. 1), only part of the liquid removed from its CV (l) will be transferred to the ET via the transfer line. In the absence of a leak, the remaining flow will be diverted to the vaporizer, so in (9)

$$J_{le} \rightarrow J_{le1} = -J_{vap} - J_{tr} - J_{l,leak1}. \tag{20}$$

In the vaporizer, a certain amount of LH2 is evaporated and returned to the ST, thus controlling its ullage pressure $p_{t1} = p_{v1}$. These processes are modeled by means of the following equations:

$$\dot{J}_{boil} = \begin{cases} (J_{vap} - J_{boil})/\tau_{vap}, & J_{vap} - J_{boil} > 0 \\ \\ 0, & \text{otherwise} \end{cases} \tag{21}$$

$$J_{vap} = c_{vap}\lambda_{vap}\sqrt{2\rho_l(p_{v1} - p_{vap})} \tag{22}$$

where the expression (22), which describes the mass flow through the vaporizer valve, is similar to that used for pneumatic valves [9]. The vaporizer valve position $\lambda_{vap}(t)$ is defined by the filling protocol described in Appendix B, and the nominal pressure in the output of the vaporizer vent, p_{vap}, is close to atmospheric. The vaporizer valve dimensionless parameter c_{vap} is given in Appendix C.

In accordance with (20), the energy transfer term on the left side of Eq. (16) should be rewritten as follows:

$$J_{le}(h_l + v_{le}^2/2) \rightarrow J_{le1}h_{l1} - J_{vap}v_{vap}^2/2 - J_{tr}v_{tr}^2/2 - J_{l,leak1}v_{l,leak1}^2/2. \tag{23}$$

The external mass flow in Eq. (10) is related to the vapor CV in the ST:

$$J_{ve} \rightarrow J_{ve1} = J_{boil} - J_{v,valve1} - J_{v,leak1}. \tag{24}$$

Similarly, in (13),

$$J_{ve}(h_v + v_{le}^2/2) \rightarrow J_{ve1}h_{v1} + J_{boil}v_{boil}^2/2 - J_{v,valve1}v_{v,valve1}^2/2 - J_{v,leak1}v_{v,leak1}^2/2. \tag{25}$$

E. The External Tank

After ascribing a subscript $i = 2$ to all relevant functions, variables, and parameters in Equations (3) – (19), we also substitute the external mass flow rate in (9) with

$$J_{le} \rightarrow J_{le2} = J_{tr} - J_{l,leak2} - J_{w/boil} \tag{26}$$

where an additional term $J_{w/boil} = \dot{Q}_{le2}/h_{lv} \propto T_{w2} - T_l$ is introduced that is responsible for intense LH2 evaporation as the ET walls are being initially chilled down during the beginning of the slow fill stage (see Eq. (17)). Then the energy transfer term on the left side of Equation (16) is to be rewritten as

$$J_{le}h_l + v_{le}^2/2 \rightarrow J_{le2}h_{l2} + J_{tr}v_{tr}^2/2 - J_{l,leak2}v_{l,leak2}^2/2. \tag{27}$$

Here, the external GH2 mass flow in Eq. (10) related to the vapor CV in the ET,

$$J_{ve} \rightarrow J_{ve2} = -J_{v,valve2} - J_{v,leak2}, \tag{28}$$

should be supplemented with that of GHe in Eq. (11),

$$J_{ge} \rightarrow J_{ge2} = J_{g,in} - J_{g,valve2} - J_{g,leak2}, \tag{29}$$

and with the subsequent modification of the energy flow term $J_{v(g)e}(h_{v(g)e} + v_{v(g)e}^2/2)$ on the left side of Eq. (13), which is similar to (23).

Ignoring the hydrostatic pressure, the mass flow rate of the leaking liquid can be estimated by means of the Bernoulli equation [5, 9]:

$$J_{l,leak} = S_{l,leak}\sqrt{2\rho_l(p_v + p_g - p_{atm})} \tag{30}$$

To find the mass flow rate of the leaking mixture of vapor and gas we use average parameters $c_{P(V)}$ and $\gamma = c_P/c_V$ for the mixture. Also, we will treat the flow as choking through a nozzle of a minimal cross

section $S_{v,leak}$ so that [5, 12]

$$J_{v(g),leak} = \frac{\rho_{v(g)} \sqrt{\gamma(p_v + p_g)}}{\Gamma \sqrt{\rho_v + \rho_g}} S_{v,leak} \tag{31}$$

where $\Gamma = ((\gamma + 1)/2)^{(\gamma+1)/2(\gamma-1)}$.

Similarly, for the vent valve k [9],

$$J_{v(g),valvek} = \frac{\rho_{v(g)} \lambda_k \sqrt{\gamma(p_v + p_g - p_{atm})}}{\Gamma \sqrt{K_k (\rho_v + \rho_g)}} S_{v,valvek} \tag{32}$$

Here, the dimensionless flow coefficient K (the loss factor) can be found in Schmidt *et. al.* [9] (see Tables 7-2 and 7-3 therein); a dimensionless relative valve position assumes values between $\lambda_k = 1$ (fully open) and $\lambda_k = 0$ (fully closed) [9].

A term $\dot{Q}_{v,leak2}$, which is responsible for an additional thermal leak in the ullage space of the ET, can be added to the right side of Equation (19).

F. Transfer Line

Let us consider a simplified version of the transfer line (TL) that connects the two tanks in the LH2 propellant loading system (Fig. 1). It will allow us to describe all the essential stages of the loading process.

In accordance with previous work [5, 9–11], we will use the following equation to relate the mass flow rate J_i through an element k of the TL with the pressure drop across it, Δp_k:

$$J_k = \alpha_k (\Delta p_k)^{1/2} \tag{33}$$

Here, similar to Eq. (32) for the (pneumatic) valve [9, 11],

$$\alpha_k = \lambda_k S_k \left(\frac{2\rho_l}{K_k} \right)^{1/2} \tag{34}$$

For a pipe of radius R, length l, and wall roughness d_r with the turbulent regime of flow ($\text{Re} \geq 3 \cdot 10^3$) [5, 10], the flow rate is given by (33) where

$$\alpha = \alpha_{pipe} = 2\pi R^2 \left(\frac{\rho_l R}{fl} \right)^{1/2} \tag{35}$$

Here, the dimensionless resistance coefficient f can be found from the Colebrook equation [10]:

$$\frac{1}{\sqrt{f}} = -0.87 \log \left(\frac{d_r}{7.4R} + \frac{2.51}{\text{Re}\sqrt{f}} \right) \tag{36}$$

15

For the laminar flow in the pipe ($Re < 3 \times 10^3$):

$$J = k_{pipe} \Delta p, \tag{37}$$

where [5]

$$k_{pipe} = \frac{\pi R^4}{8 \nu l}. \tag{38}$$

The total pressure drop across the TL is the sum of all the pressure drops across the line:

$$\Delta p_{tot} = \sum \Delta p_k = p_{v1} - p_{v2} - p_{g2} + \rho_l g (h_{l1} - h_{l2}), \tag{39}$$

where the levels of liquid h_{l1} and h_{l2} of LH2 in both tanks are counted from the same level. For the sake of simplicity, here we ignore the friction pressure drops in the pipes connecting the valves with the main line, considering the latter as a straight pipe. Then, assuming the flow is turbulent in all of the elements of the TL, including the main cross-country line (the pipe) ($Re_{pipe} > Re_{cr} \approx 10^3$), the steady (nominal) mass flow rate in the TL can be easily calculated as

$$J_{tr}^{(st)} = \alpha_{eff} \Delta p_{tot}^{1/2} \tag{40}$$

For the chosen model of the TL (see Fig. 1),

$$\alpha_{eff} = \left(\alpha_V^{-2} + \alpha_{pipe}^{-2} \right)^{-1/2}, \tag{41}$$

where

$$\alpha_V = \left[(\alpha_E + \alpha_F)^{-2} + (\alpha_J + \alpha_K)^{-2} + \alpha_L^{-2} + (\alpha_M + \alpha_N)^{-2} \right]^{-1/2}. \tag{42}$$

It can be seen that in this case, the mass flow rate (40) in the TL resembles that of a straight pipe with the turbulent regime.

If the flow in the cross-country line is laminar ($Re < Re_{cr} \approx 10^3$), then using (28), (32), and (34) yields

$$J_{tr}^{(st)} = \frac{\alpha_V^2}{2k_{pipe}} \left[\sqrt{1 + \frac{4k_{pipe}^2 \Delta p_{tot}}{\alpha_V^2}} - 1 \right], \tag{43}$$

where α_V is given by (42). Here the mass flow rate dependence on the total pressure drop (39) is sub-linear.

The transient flow through the TL can be found from the equation:

$$\dot{J}_{tr} = \left(J_{tr}^{(st)} - J_{tr} \right) / \tau_{tr}, \tag{44}$$

where the steady (nominal) flow rate is given by either (40) or (43).

16

G. Summary of the Model

Our reduced LH2 loading model can be summarized as follows. There are 20 time-dependent state variables: $m_{li}, m_{vi}, m_{g2}, p_{vi}, p_{g2}, V_{vi}, T_{li}, T_{vi}, T_{fi}, T_{wi}, J_{boil}$, and J_{tr} with $i = 1, 2$. There are 7 constraints that include: (*i*) 2 equations of state for LH2 in both the ST and ET and 1 equation of state for GHe in the ET (see Eq. (7)), (*ii*) 2 equations of state (8) for the vapor film in both tanks, and (*iii*) 2 equations (12) relating the vapor/gas volume to the LH2 mass and to the total volume for both tanks. There are $13 = 20 - 7$ time-dependent ordinary integro- (in the presence of the conduction term (3)) differential equations that include: (*i*) 5 mass conservation equations for LH2 (9) and GH2 (10) in both tanks as well as for GHe (11) in the ET, (*ii*) 4 energy conservation equations for GH2/GHe (13) and LH2 (16) in both tanks, (*iii*) 2 energy conservation equations (19) for the tank walls, and (*iv*) 2 rate equations, (21) and (44), that govern the mass flow rate delivered from the vaporizer and that of the transfer line. The rest of the dynamical variables responsible for the vent valve positions (and different leaks) are governed by the filling protocol (see Appendix B).

IV. Nominal Propellant Loading Regime

First, we will apply the presented reduced model to describe a multi-stage nominal LH2 loading regime. Filling progresses in several stages: pressurization, slow fill, fast fill, fast fill at reduced pressure, reduced-flow fast fill, topping, and replenish (see Appendix B for additional details).

The fill operation starts with pressurization. Initially, there is no flow path between the tanks. The initial ullage temperature for the ST is assumed to be 20 K, which is the equilibrium saturated gas temperature at the initial pressure of 1.01×10^5 Pa (1 atm). The initial ullage temperature for the ET is known from data to be around 300 K. The tanks are individually pressurized before any transfer of LH2 is initiated. The ST is filled with a large amount of LH2 while the ET has none, and both tanks are filled with enough GH2 for an ullage pressure equal to atmospheric pressure. The ST is pressurized first to about 3.77×10^5 Pa, and then to 5.56×10^5 Pa solely through the use of the vaporizer. The vaporizer valve opens, allowing LH2 to flow through the vaporizer, which boils off LH2, and the created GH2 feeds back into the ST. Concurrently, the ET is pressurized to 2.67×10^5 Pa by using GHe fed in through the pre-pressurization valve.

After pressurization is complete, slow fill begins. The transfer line chilldown valve, main fill valve, outboard fill valve, inboard fill valve, and topping valve are all opened. The ullage pressure in the ST, which

is constantly maintained by the vaporizer, drives fluid to the ET. The flow through the vaporizer valve is modulated based on the error between the measured ST ullage pressure and the ST pressurization set point. The ullage pressure in the ET is maintained using its vent valve, which opens and closes to maintain the pressure between 2.67×10^5 and 2.88×10^5 Pa.

Fast fill begins when the ET is 5% full. The transfer line valve opens to increase flow from about 5.68 m^3/min to around 28.4 m^3/min. Fast fill at reduced pressure starts when the ET is 72% full. The ullage pressure of the ST is reduced to 4.46×10^5 Pa, through control of the vaporizer valve. When the ET is 85% full, fast fill at a reduced flow rate begins. The main fill valve is set at a reduced flow state.

When the ET is 98% full, topping begins. The transfer line valve is closed and the replenish valve J fully opens. The ET vent valve is also opened, reducing the ET ullage pressure to 1.01×10^5 Pa. The inboard fill valve closes, forcing the remaining liquid to pass into the ET through the topping valve. Finally, at 100% full, topping ends and the tank is continuously replenished to replace the boil off before launch. During replenish, the transfer line chilldown valve remains open, the main fill valve is closed, and the replenish valve is modulated to maintain the ET level at 100%.

Fig. 4 summarizes the major results of the simulation of a nominal loading regime, which are based on the parameters, initial conditions, and a filling protocol that all are typical for LH2 loading systems (see Appendix C).

It can be seen (Fig. 4a) that the LH2 level in the ST drops monotonically as the level in the ET rises (Fig. 4d). The pressure p_1 in the ST (Fig. 4b) is determined by the loading dynamics (filling protocol) and controlled by the vaporizer and vent valves. It should be noted here that, once achieved during slow fill, the pressure in the ST is maintained at approximately 5.56×10^5 Pa up to the end of the reduced-pressure fast fill (see Figs. 4b and 4j), at which point it is maintained at 4.46×10^5 Pa. Meanwhile, the ET ullage pressure (Fig. 4e) is oscillating due to the cycling of the vent valve that maintains the pressure between lower and upper thresholds of 2.67×10^5 and 2.88×10^5 Pa, correspondingly. The fluctuations in the ET ullage temperature (Fig. 4f) as well as in the mass flow rates (Figs. 4j and 4h) are driven by the ET pressure oscillations. (The nontrivial dynamics of these on-off oscillations will be discussed later on.)

The LH2 partial pressure in the ET rises due to the continuing hydrogen supply, while the GHe partial pressure drops because the helium is being permanently removed through the vent valve (Fig. 4i). In this case,
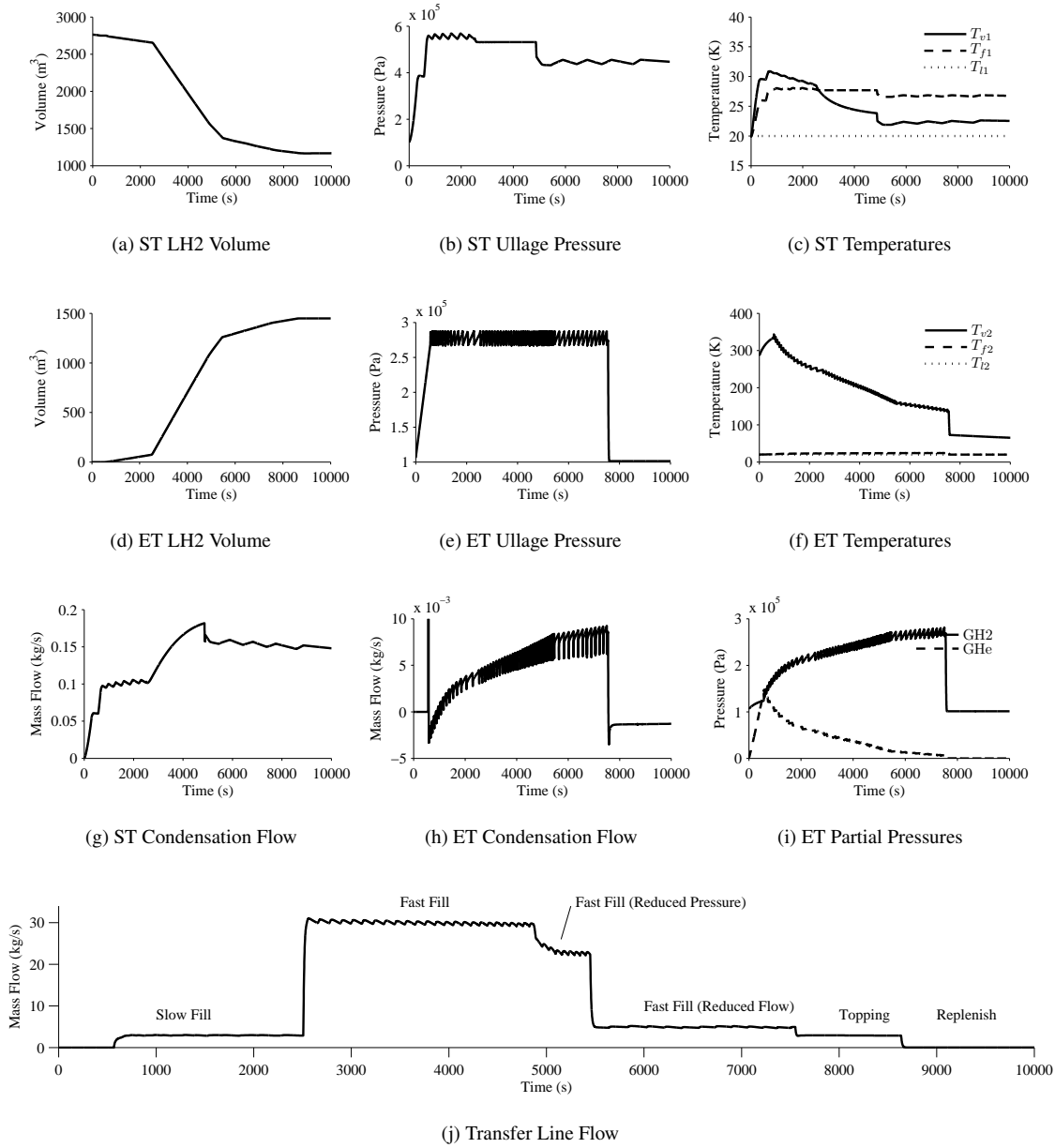
(a) ST LH2 Volume

(b) ST Ullage Pressure

(c) ST Temperatures

(d) ET LH2 Volume

(e) ET Ullage Pressure

(f) ET Temperatures

(g) ST Condensation Flow

(h) ET Condensation Flow

(i) ET Partial Pressures

(j) Transfer Line Flow

Fig. 4 Nominal regime of LH2 propellant loading.

due to the condensation blocking effect [4], the flow of the condensed vapor in the ET (Fig. 4h) is several orders of magnitude smaller than that in the ST (Fig. 4g), because the vapor pressure is being maintained approximately equal to the equilibrium pressure of the condensed vapor at the temperature of LH2. The ullage temperature T_{v2} in the ET (Fig. 4f) increases initially due to the introduction of the GHe during the pressurization stage, then drops from the initial high value due to venting and near-wall boiling that generates relatively cold GH2 during filling. The liquid surface temperature T_{f1} in the ST increases (Fig. 4c) due to the vapor condensation at the v/l-interface (see Fig. 2b). Simultaneously, the ST ullage temperature T_{v1}

increases, mainly because the relatively hot GH2 is supplied by the vaporizer as loading is going on. As a result, the ullage temperature approaches the temperature of LH2 saturated vapor at a pressure close to the final ST ullage pressure of approximately 5.06×10^5 Pa (5 atm) (Fig. 4b).

V.   Loading Regime Faults

In this section we analyze how different deviations from the nominal regime (faults) would affect the LH2 loading dynamics. In principle, this would enable us to identify what sensor data can be utilized for fault diagnostics and prognostics.

A.   Gas Leak Faults

We define the gas leak fault as an opening of a hole with effective cross-sectional area $S_{v,leak}$ in the ullage part of one of the tanks, which gives rise to an additional gas flow described by Eq. (31). Figs. 5 and 6 show how the introduction of such leaks at $t = 30$ min affects the history of both tanks. The leak in the storage tank (Fig. 5), being noticeable at large enough cross-sectional areas $S_{v,leak1} \geq 1 \times 10^{-3}$ m^2, will affect all the dynamic characteristics in both tanks immediately after its initiation. Due to the leak, it is more difficult for the ST ullage pressure to be maintained with the vaporizer. For $S_{v,leak1} = 3 \times 10^{-3}$ m^2, the leak size is large enough to cause a drop in p_1 at the initiation of fast fill. As a result, loading takes a longer time, as shown in Figs. 5a and 5d. Therefore, the topping stage, at which the ET vent valve remains open, is arrived at later, which is why for $S_{v,leak1} = 3 \times 10^{-3}$ m^2, the drop in p_2 to atmospheric pressure occurs about 200 seconds later than in the nominal scenario.

A leak of similar size in the ET has much more dramatic consequences, i.e. a leak of size $S_{v,leak2} = 1 \times 10^{-3}$ m^2 is large enough that the ET ullage pressure cannot be maintained above its lower threshold during filling, requiring an abort. Therefore, we consider faults of size an order of magnitude less. It can be seen that leaks in the ET do not noticeably affect most variables (Fig. 6). However, the presence of gas leaks can be detected almost immediately after their initiation at $t = 30$ min by observing the rate at which the ullage pressure increases and decreases as it oscillates between the limits set by the vent valve thresholds (Fig. 7). In particular, the ET pressure increases more slowly in the presence of the gas leak, so the vent valve-generated pressure oscillations lag behind those of the nominal regime. As a result, the vent valve cycling frequency at all times decreases with the introduction of the leak compared to the nominal one
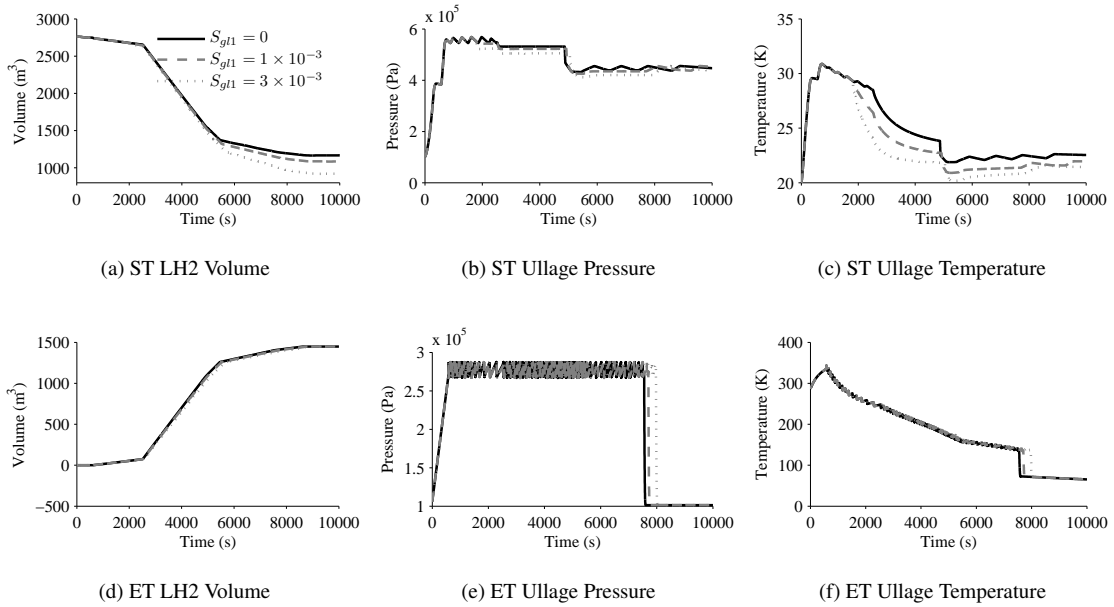
(a) ST LH2 Volume   (b) ST Ullage Pressure   (c) ST Ullage Temperature

(d) ET LH2 Volume   (e) ET Ullage Pressure   (f) ET Ullage Temperature

Fig. 5 Effects of gas leak in the ST on the LH2 level, vapor temperature, and ullage pressure as functions of time in ST and ET.

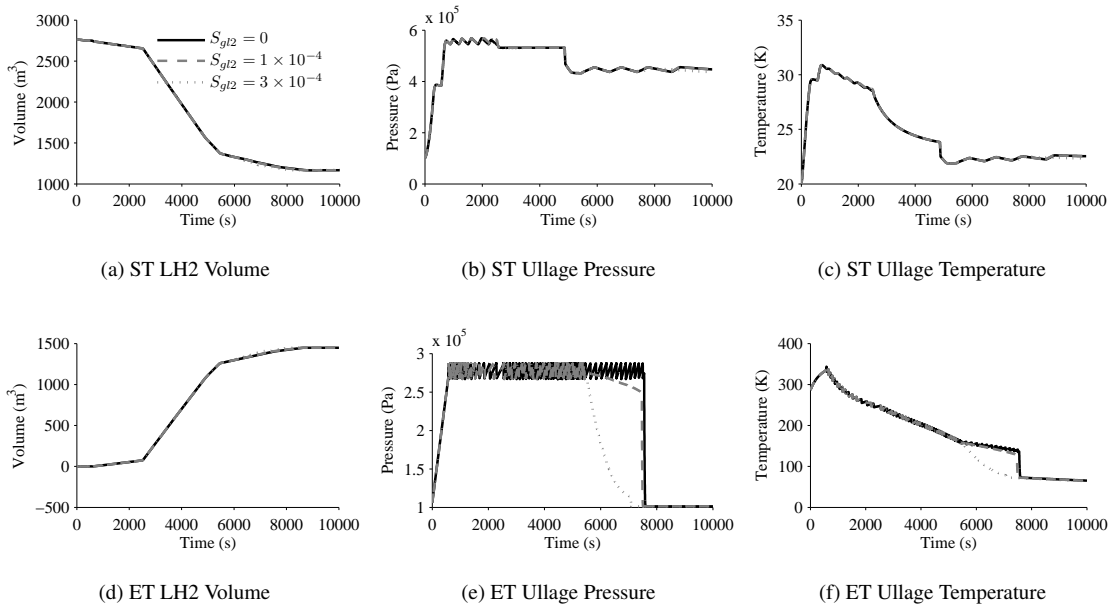(a) ST LH2 Volume   (b) ST Ullage Pressure   (c) ST Ullage Temperature

(d) ET LH2 Volume   (e) ET Ullage Pressure   (f) ET Ullage Temperature

Fig. 6 Effects of gas leak in the ET on the LH2 level, vapor temperature, and ullage pressure as functions of time in ST and ET.

(Fig. 8). It can be seen that the frequency itself, with or without gas leaks, changes non-monotonically with time. Its initial drop is due to the decreasing rate of boiling in the ET and to the decrease in the corresponding pressure buildup. The subsequent increase in frequency can be attributed to the reduction in the ullage space
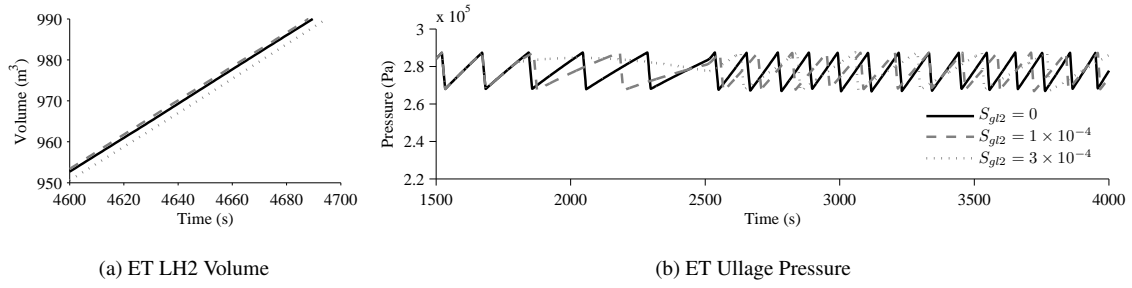
(a) ET LH2 Volume   (b) ET Ullage Pressure

Fig. 7 Effects of ET gas leak of different size (in m^2) on the LH2 level and the ullage pressure oscillations in the ET.
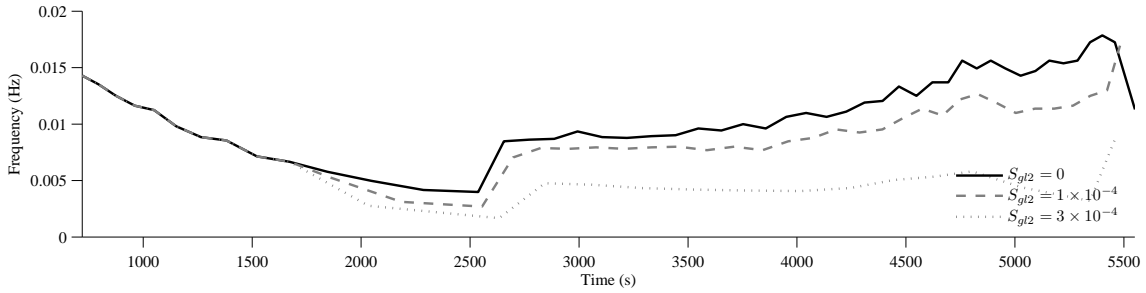

Fig. 8 Effects of ET gas leak on its vent valve open/close frequency. The frequency is computed as the inverse of the time difference between the pressure peaks.

that allows for faster changes in pressure.

B.   Vent Valve Clogging Fault in the ET

The clogging fault is defined as a substantial decrease in the vent valve cross-section $S_{v,valve2}$ quantified by a multiplicative clogging factor $\sigma_{S_{valve2}}$. It can be seen (Fig. 9) that its effect is relatively small, so the loading can still be accomplished in spite of a significant (up to 75%, for $\sigma_{S_{valve2}} = 0.25$) ET vent valve clogging assuming $S_{v,valve2}^{(\mathrm{nominal})} = 0.025\mathrm{m}^2$. Additional simulations have confirmed that a full clog leads to a significant ET ullage pressure buildup that requires aborting the fueling operation. Figure 10 shows that though loading is slightly slower when the ET vent valve clogs, it can be detected, similar to the gas leak, by observing a difference in the pressure relief rate, and, correspondingly, a decrease in vent valve frequency.
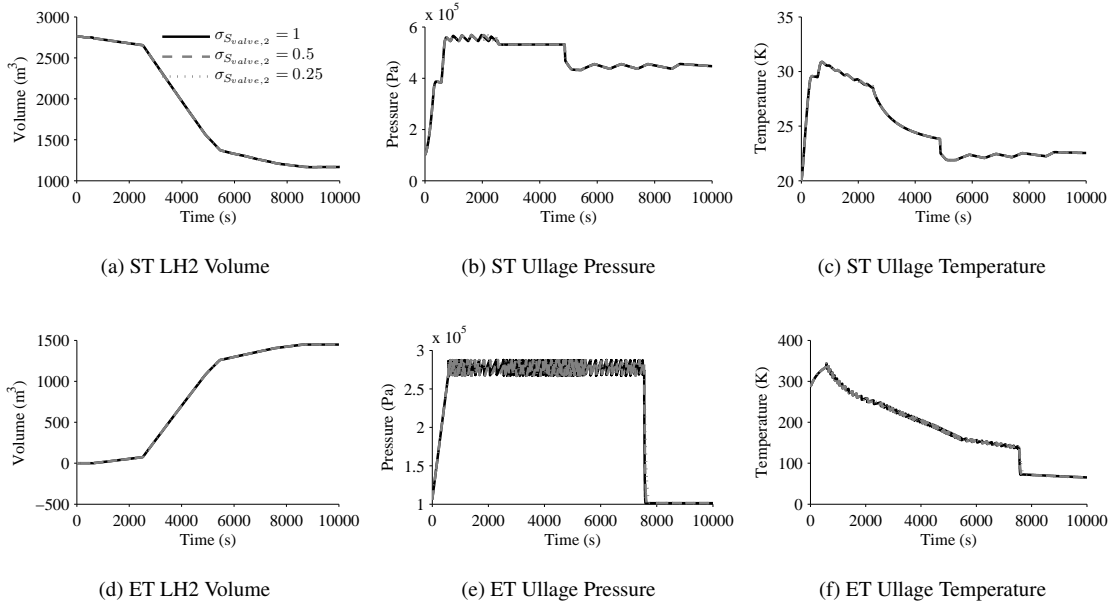
(a) ST LH2 Volume   (b) ST Ullage Pressure   (c) ST Ullage Temperature

(d) ET LH2 Volume   (e) ET Ullage Pressure   (f) ET Ullage Temperature

Fig. 9 Effects of ET vent valve clogging fault on the LH2 level, temperature, and ullage pressure as functions of time in the ST and the ET.
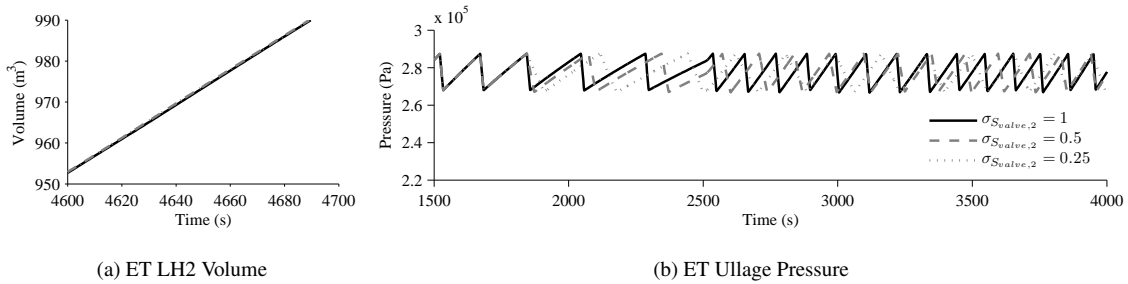

(a) ET LH2 Volume   (b) ET Ullage Pressure

Fig. 10 Effects of ET vent valve clogging on the LH2 level and the ullage pressure oscillations in the ET.

VI.   Comparison with the Shuttle Loading System Data

The ultimate verification of any model lies in its ability to adequately describe real systems. We have checked our reduced dynamical model against real historical data for the LH2 Shuttle loading system (Fig. 11). Here, when simulating basic processes and finding time-dependent characteristics, we used a set of typical system parameters, and used commanded valve positions as inputs.

It can be seen that the results of our modeling are in reasonable agreement with the real data, especially for the ST (Fig. 11a). It should be noted here that the amount of LH2 in the ST depends largely on the two factors: (*i*) the transmission line mass flow rate flow rate and (*ii*) the vaporizer mass flow rate, governed by Eqs (44) and (21), respectively. (The model takes those factors into consideration quite appropriately.)
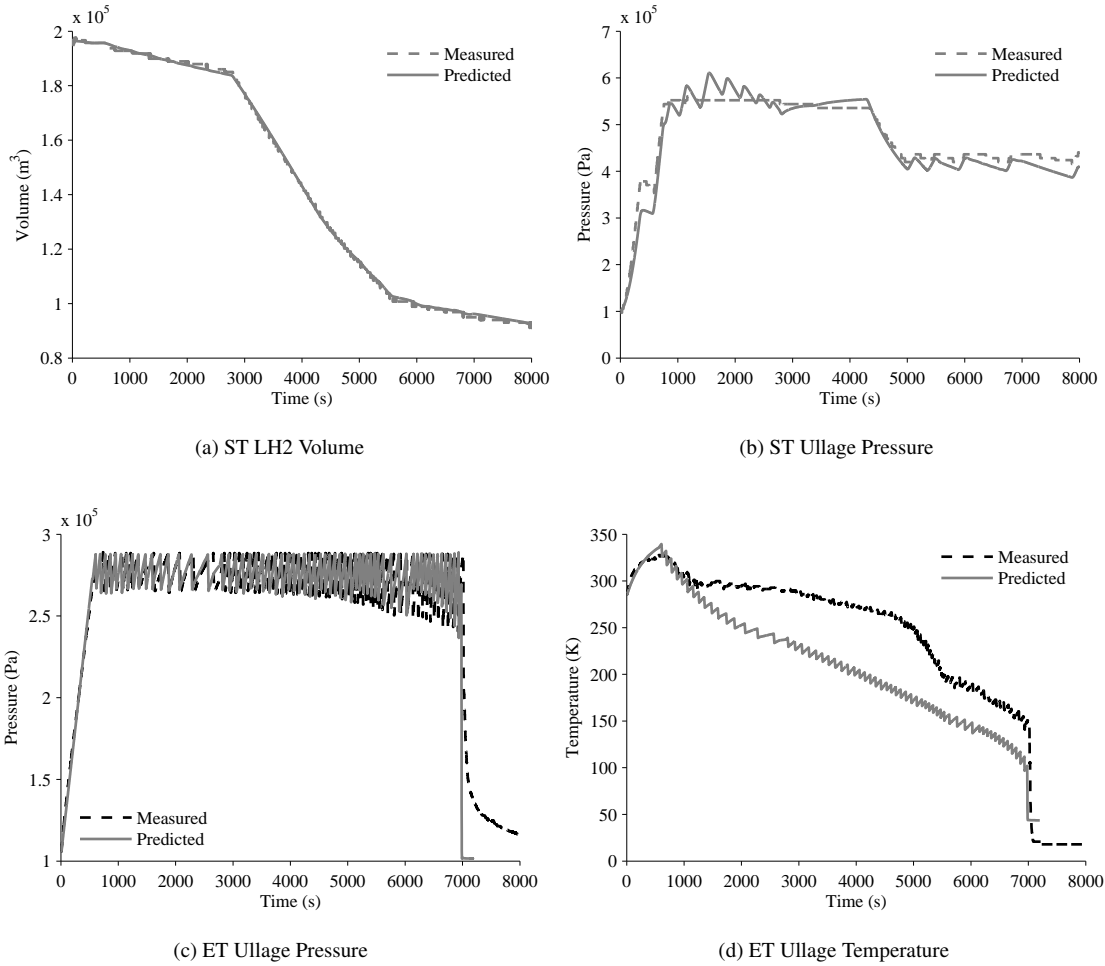
(a) ST LH2 Volume

(b) ST Ullage Pressure

(c) ET Ullage Pressure

(d) ET Ullage Temperature

Fig. 11 Comparison of the results of simulations with real data on ST and ET history.

Meanwhile, the ST ullage pressure is mainly controlled by the vaporizer mass flow rate. The errors observed in the predicted ST ullage pressure are due to the lack of knowledge on specific vaporizer parameters and the continuous position of the vaporizer valve. Only the discrete position of the valve was known, so when the valve was partially open the exact position was unknown. During this time we assumed the vaporizer valve behaved as described in Appendix B, where the valve position is controlled based on the error between the actual and desired ST ullage pressures.

In addition, our model allows for a fairly adequate description of the ET ullage history (Figs. 11c and 12a). Here, the ET ullage pressure is regulated by the ET vent valve, whereas the rate of pressure changes is governed by several factors, namely by: (*i*) the TL mass flow rate, (*ii*) the LH2 boiling in the vicinity of the ET walls, which is especially intensive in the beginning of the filling process, (*iii*) the evaporation/condensation rate, and (*iv*) the vent valve behavior (Fig. 11c). A comparison of the vent valve open/close
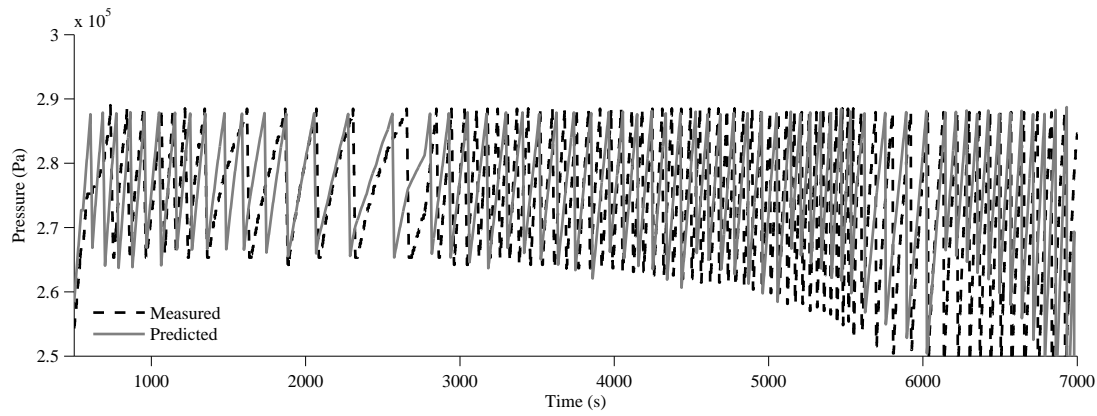
(a) ET Ullage Pressure
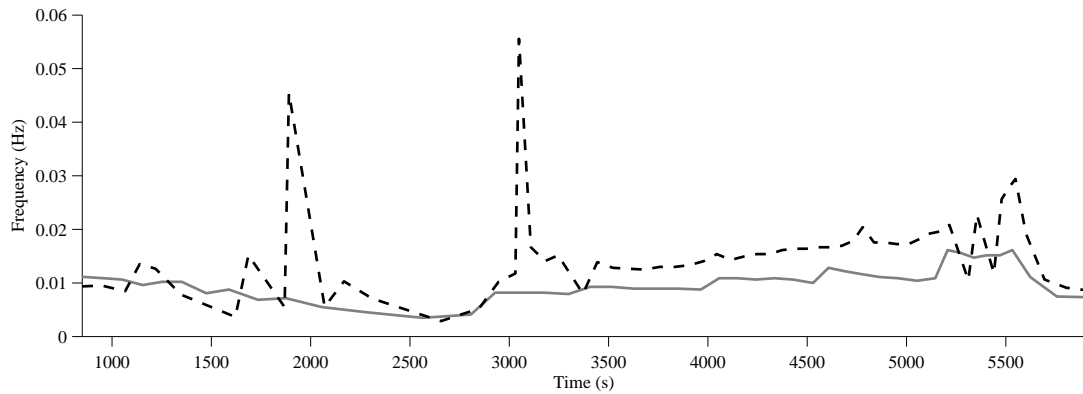
(b) ET Vent Valve Frequency

Fig. 12 Comparison of the results of simulations with real data on ET ullage pressure and vent valve frequency.

frequency is shown in Fig. 12b. The differences in frequency may be attributed to our approximate description of LH2 boiling in the ET that is a result of ET chilling. The spikes in measured frequency occur at transitions of the filling rates and at transitory boiling events, which disrupt the regularity of the valve switching. Because the ET begins at ambient temperature, it is chilled down only during filling. The LH2 boiling near the ET walls is crucial to explaining the increased rate of pressure oscillations during slow fill, as the rate of pressure increase cannot be described solely by the TL mass flow rate and the estimated evaporation/condensation rate.

Our model correctly describes the initial rise in the ET temperature (Fig. 11d) that happens due to the GHe pressurization. A subsequent cooling is apparently driven by (*i*) the tank's chilling down, (*ii*) the supply of the relatively cold hydrogen vapor due to boiling, and (*iii*) the release of vapor through the vent valve. Here the discrepancy between the results of our simulations and the experimental data is pretty visible. We

25

attribute this to a substantial temperature stratification [13, 14] that happens in the upper-stage cryogenic tanks (ET) and to the unknown position of the sensor that measures a local ullage temperature shown in Figure 11d. Despite these shortcomings the proposed model adequately describes the rate of mass flow through the transfer line (TL). The reason is that this rate is governed by the pressure difference in both tanks as well as by the effective varying (nonlinear) hydraulic resistance of the (TL). The model apparently captures the above features of the LH2 loading system.

A correct theoretical description of the ET ullage pressure history due to the valve on-off oscillations is a quite challenging task [15]. Its importance for diagnostics and prognostics purposes has been mentioned in Section V. Our model handles this problem rather well (Fig. 11c). It can be seen that though the theoretically predicted oscillations initially lose their phase relative to experimental ones due to transient boil-off events in the ET, once the transient decays, the phase of oscillations is recovered and the theoretical model predicts real data fairly well. The predicted frequency during fast fill is a bit below the measured frequency, and this is attributed to some transitory boiling still occurring at the tank walls during fast fill. Such behavior may be better captured by breaking up the tank wall CV into multiple CVs.

VII.   Conclusions

We developed a dynamical model for a complex spatially-distributed system of LH2 loading that involves the storage and external tanks as well as the transfer line. The proposed reduced model is based on a set of coupled ordinary integro-differential equations for the state variables, which is shown to be well suited to describing the generic cryogenic loading system, including the one currently used for Shuttle fueling in both the nominal and major faulty regimes. The model accounts for the pressurizing helium gas injected in the ET and can be easily modified for similar cryogenic propellant loading systems.

The main results of this work include the following. First, we incorporate highly non-equilibrium condensation-evaporation processes at the vapor/liquid interface of the LH2 tanks for the sake of adequate description of the systems for the propellant loading of liquid-fuel rockets. Contrary to previous considerations [1–3], the present model, in a self-consistent manner, accounts for different modes of the interfacial heat exchange (see Fig. 2). Second, we successfully reduce the above description to a low-dimensional performance model comprising a compact set of ordinary integro-differential equations. Those allowed us to

incorporate non-trivial interaction between spatially distributed parts of a generic loading system, such as the vaporizer, both tanks, and the cross-country line. Third, we develop numerical algorithms applicable to accurate analysis of the generic nominal loading regime and of the effects of possible faults. Last, we analyze both the nominal regime and the most probable faults to be further utilized for fault diagnostics and prognostics.

We have analyzed the effects of several primary faults, such as gas leaks in the ullage space of both the ST and ET, as well as clogging of the ET vent valve, on the history of both tanks. We found that each of the faults is characterized by quite pronounced dynamics. The most interesting new observation is that some of the faults, such as a substantial clogging of the ET vent valve or a leak in the ET ullage volume, usually have a slight effect on the integral variables, namely on the volumes of LH2 in the tanks or even on the ullage temperatures and pressures, yet the dynamics of the vent valve-induced pressure oscillations are shown to be extremely sensitive even to small deviations from the nominal regime and can be used for early fault identification by means of real-time sensor data analysis. Using the model, we propose to not only identify different faults based on the analysis of the sensor data characterizing the filling dynamics, but also infer the parameters of the model to be further used for prediction of future behavior of the system.

By introducing additional control volumes in the ullage space of the tanks, similar to what has been done in [14], it is possible to extend our model to account for the effects of the ullage temperature stratification. The work on this subject is currently underway.

Appendix A: Convection Heat Transfer Coefficients

We will follow Schmidt *et al.* [9] in defining the natural-convection heat transfer coefficient for a vertical isothermal wall as:

$$\alpha_{ve} = \frac{\text{Nu}_L \cdot \kappa_{v(l)}}{L_{v(l)}} \tag{45}$$

where $L = L_{v(l)}$ is the height of the wall in contact with vapor or liquid, which for the ET can be estimated as:

$$L_l = h_{l2} = m_{2l}/\rho_l; L_v = H_2 - h_{l2} = H_2 - m_{2l}/\rho_l \tag{46}$$

In (45) the average dimensionless Nusselt number

$$\mathrm{Nu}_L = 0.68 + 0.503 \left[\mathrm{Ra}_L \cdot \Psi\right]^{1/4} \tag{47}$$

where the dimensionless Rayleigh number

$$\mathrm{Ra}_L = \frac{g\beta \left(T_w - T_{v(l)}\right) L_{v(l)}^3 \mathrm{Pr}_{v(l)}}{\nu_{v(l)}^2} \tag{48}$$

with the volumetric expansion coefficient β for gases being close to $1/T_v$ and the dimensionless Prandtl number

$$\mathrm{Pr}_L = \frac{c_{P(l)}\mu_{v(l)}}{\kappa_{v(l)}} \tag{49}$$

and

$$\Psi = \left[1 + \left(\frac{0.492}{\mathrm{Pr}_L}\right)^{9/16}\right]^{-16/9} \tag{50}$$

For the ST the LH2 volume

$$V_{l1} = \frac{\pi}{3}h_{l1}^2(3R_1 - h_{l1}) \tag{51}$$

and the l/v interface area

$$A_1 = \pi \left(R_1^2 - (R_1 - h_{l1})^2\right). \tag{52}$$

For the ET, $V_{l2} = A_2 h_{l2}$, $A_2 = \pi R_2^2$, $A_{l2} = 2\pi R_2 A_2 h_{l2}$, and $A_{v2} = 2\pi R_2 A_2(H - h_{l2})$. For the spherical ST, the heat transfer between a sphere and the fluid it encloses $\mathrm{Nu}_d = 0.098\mathrm{Ra}_d^{0.345}$ to be used, while for the heat transfer from the horizontal film (liquid) to the vapor in both cases $\mathrm{Nu}_d = 0.14\mathrm{Ra}_d^{0.333}$ (see [1, 9]] where is to be used.

Appendix B: Filling Protocol

The protocol of Table 1 describes sets of the valve positions λ_k (see Eqs (32) − (34)) that fully define the filling regimes. The valve notations k can be found in Figure 1, e.g., E corresponds to the transfer line valve. Here, correspondingly for the replenish and ET vent valve positions,

$$f_{repl}\left(h_{l2}\right) = \begin{cases} 0, & h_{l2} > H_2 \\ 1, & \min\left(1, 0.1\frac{0.999H_2 - h_{l2}}{0.999H_2}\right) \end{cases} \tag{53}$$

Table 1 Filling Protocol Valve Positions

	A E F	J	K L M N	ET Vent	p_1^*
Pressurization	1 0 0	0	1 1 1 0	$f_{vent,2}(p_2)$	p_{press}
Slow Fill	0 0 1	0	1 1 1 1	$f_{vent,2}(p_2)$	p_{slow}
Fast Fill	0 1 1	0	1 1 1 1	$f_{vent,2}(p_2)$	p_{fast}
Fast Fill (Red. Press.)	0 1 1	0	1 1 1 1	$f_{vent,2}(p_2)$	$p_{reduced}$
Fast Fill (Red.Flow)	0 1 1	1	0.1 1 1 1	$f_{vent,2}(p_2)$	$p_{reduced}$
Topping	0 0 1	1	0.1 1 0 1	1	$p_{topping}$
Replenish	0 0 1	$f_{repl}(h_{l2})$	0 1 0 1	1	$p_{replenish}$

and

$$f_{vent,2}\left(p_2\right) = \begin{cases} 0, & p_2 - p_{2,low} \\ 1, & p_2 - p_{2,high} \\ \lambda_{vent,2}^-, & otherwise \end{cases} \tag{54}$$

where λ_k^- refers to the previous value of λ.

For the ST vent and vaporizer valves, the vent positions λ are described correspondingly by

$$f_{vap}\left(p_1, p_1^*\right) = \begin{cases} \min\left(1, \max\left(0, 10\left(\left(p_1^* - p_1\right)/p_1^*\right)\right)\right), & p_1 < 0.98 p_1^* \\ 0, & p_1 > 1.02 p_1^* \\ \lambda_{vap}^-, & otherwise \end{cases} \tag{55}$$

and

$$f_{vent,1}\left(p_1, p_1^*\right) = \begin{cases} 0, & p_1 < 1.05 p_1^* \\ 1, & p_1 > 0.95 p_1^* \\ \lambda_{vent}^-, & otherwise \end{cases} \tag{56}$$

Here, p_1^* refers to desired values of pressure in the ST that are specified in the last column of the above table.

Simulation parameter values are given in Table 2. Many of the system parameters values were derived directly from system documents. The remaining parameters were estimated from system data, including τ_{vap}, c_{vap}, $\alpha_{l,e}$, τ_{tr} and each of the K_k values for $k \in \{E, F, J, K, L, M, N\}$ (see Fig. 1). The position of the main fill valve K in its reduced flow state during fast fill (reduced flow) and topping was also estimated from data.

Table 2 Parameter Values

Hydrogen and Helium	$T_c = 33.2$ K, $p_c = 1.315 \times 10^6$ Pa, $\lambda = 5$, $\rho_L = 71.1$ kg/m^3, $c_L = 9450$ J/kg/K,
	$\kappa_L = 0.0984$ W/m/K, $h_{lv}^0 = 4.47 \times 10^5$ J/kg, $\mu = 3.4 \times 10^{-6}$ Pa s, $R_v = 4124$ J/kg/K,
	$c_{V,v} = 6490$ J/kg/K, $\gamma = 5/3$, $\kappa_v = 0.0166$ W/m/K, $R_g = 2077$ J/kg/K,
	$\kappa_g = 0.0262$ W/m/K, $c_{V,g} = 3121$ J/kg/K, $c_{P,g} = 5193$ J/kg/K
Storage Tank	$R_1 = 9.16$ m, $\tau_{vap} = 20$ s, $c_{vap} = 5.89 \times 10^{-4}$, $S_{valve,1} = 0.025$ m^2
External Tank	$R_2 = 8.41$ m, $H_2 = 26.96$ m^2, $\alpha_{l,e} = 8.0$ W/m^2/K, $m_w c_w = 5 \times 10^5$ J/K,
	$S_{valve,2} = 0.05$ m^2
Transfer Line	$D_{pipe} = 0.254$ m, $l_{pipe} = 457.2$ m, $d_r = 1 \times 10^{-6}$, $\tau_{tr} = 10$ s,
	$S_E = 0.1013$ m^2, $K_E = 4$, $S_F = 0.1459$ m^2, $K_F = 1 \times 10^5$, $S_J = 0.0041$ m^2, $K_J = 66$,
	$S_K = 0.0643$ m^2, $K_K = 140$, $S_L = 0.0643$ m^2, $K_L = 0.11$, $S_M = 0.0643$ m^2, $K_M = 0.11$,
	$S_N = 0.0643$ m^2, $K_N = 0.38$

References

[1] Estey, P. N., Lewis Jr., D. H., and Connor, M., "Prediction of a Propellant Tank Pressure History Using State Space Methods," *J. of Spacecraft and Rockets*, Vol. 20, No. 1, 1983, pp. 49–54.

[2] Torre, C. N., Witham J. A., Dennison E. A., McCool R. C., and Rinker, M. W., "Analysis of a Low-Vapor-Pressure Cryogenic Propellant Tankage System," *J. Spacecraft*, Vol. 26, 1987, pp. 368–378.

[3] DeFelice, D. M. and Aydelott, J. C., "Thermodynamic Analysis and Subscale Modeling of Space-Based Cryogenic Propellant Systems," NASA TM-8992, July 1987.

[4] Osipov, V. V. and Muratov, C. B., "Dynamic Condensation Blocking in Cryogenic Refueling," *Applied Physics Letters*, Vol. 93, No. 22, 2008, pp. 224105-1-4.

[5] Landau, L. D. and Lifshitz, E. M., *Fluid Mechanics*, 2nd ed., Pergamon Press, 1987.

[6] Clark, J. A., "Universal Equations for Saturation Vapor Pressure," 40th AIAA/ASME/SAE/ASEE Joint Propulsion Conference and Exhibit, Fort Lauderdale, FL, AIAA Paper 2004-4088, July 2004.

[7] Dean, J. A., *Lange's Handbook of Chemistry*, 12th ed., McGraw-Hill, New York, 1979.

[8] NIST Chemistry WebBook, NIST Standard Reference Database Number 69.

[9] Schmidt, F. W., Henderson, R. E., and Wolgemuth, C. H., *Introduction to Thermal Sciences*, 2nd ed., J. Wiley & Sons, 1993.

[10] Streeter, V. L., Wylie, E. B., and Bedford, K. W., *Fluid Mechanics*, 9th ed., McGraw Hill, 1998.

[11] Daigle, M. and Goebel, K., "Model-based Prognostics under Limited Sensing," Proceedings of the 2010 IEEE Aerospace Conference, March 2010.

[12] Osipov, V. V., Luchinsky, D. G., Smelyanskiy, V. N., Kiris, C., Timucin, D. A., and Lee, S. H., "In-Flight Failure Decision and Prognostic for the Solid Rocket Booster," 43rd AIAA/ASME/SAE/ ASEE Joint Propulsion Conference and Exhibit, Cincinnati, OH, AIAA Paper 2007-582, July 2007.

[13] Ahuja, V., Hosagady, A., Mattick, S., Lee, C. P., Field, R. E., and Ryan,H. , "Computational Analyses of Pressurization in Cryogenic Tanks," 44th AIAA/ASME/SAE/ASEE Joint Propulsion Conference and Exhibit, Hartford, CT, AIAA Paper 2008-4752, July 2008.

[14] Schallhorn, P., Campbell, D. M., Chase, S., Puquero, J., Fontenberry, C., Li, X., and Grob, L., "Upper Stage Tank Thermodynamic Modelling Using SINDA/FLUINT," 42nd AIAA/ASME/SAE/ASEE Joint Propulsion Conference and Exhibit, Sacramento, CA, AIAA Paper 2006-5051, July 2006.

[15] Grayson,G., Lopez, A., Chandler, F., Hastings, L., Hedayat, A., and Brethour, J., "CDF Modelling of Helium Pressurant Effects on Cryogenic Tank Pressure Rise Rates in Normal Gravity," 43rd AIAA/ASME/SAE/ ASEE Joint Propulsion Conference and Exhibit, Cincinnati, OH, AIAA Paper 2007-5524, July 2007.